Journal of Power Sources 195 (2010) 4772–4778

Contents lists available at ScienceDirect

Journal of Power Sources

journal homepage: www.elsevier.com/locate/jpowsour

Electrodeposition of yttria/cobalt oxide and yttria/gold coatings onto ferritic stainless steel for SOFC interconnects

Elisabetta Tondo[a], Marco Boniardi[b], Donato Cannoletta[a], Maria Federica De Riccardis[c], Benedetto Bozzini[a,*]

[a] Dipartimento di Ingegneria dell'Innovazione, Università del Salento, via Monteroni, I-73100 Lecce, Italy
[b] Dipartimento di Meccanica, Politecnico di Milano, via La Masa 34, 20156 Milano, Italy
[c] ENEA Brindisi Research Centre, SS.7 Appia Km 712, 72100 Brindisi, Italy

ARTICLE INFO

Article history:
Received 8 October 2009
Received in revised form 20 January 2010
Accepted 21 February 2010
Available online 26 February 2010

Keywords:
SOFC
Interconnect
Electrodeposition
ASR
Yttria
Chitosan

ABSTRACT

Durability seems to be the single most critical issue for the widespread application of SOFCs. Among critical issues, the stability of interconnects – operating at high temperatures in aggressive gas environments – calls for the selection of cheap materials exhibiting high corrosion performance, accompanied by low surface contact resistance. Use of coated AISI 430 stainless steel is currently the state-of-the-art choice. In this paper we propose Y_2O_3, Y_2O_3/Co_3O_4 and Y_2O_3/Au composite films as innovative coatings for AISI 430 plates. These coatings were electrodeposited from chloride salts dissolved in hydroalcoholic solutions containing chitosan as binder. The evolution of the crystalline structure of the electrodeposits with heat-treatment conditions has been studied by XRD, their chemical composition has been evaluated by EDX analysis, their morphology has been observed by SEM and the adhesion has been measured by scratch testing. Coated samples were oxidised in air at 800 °C for times up to 500 h and the area-specific resistance (ASR) as a function of exposure time has been measured. All the coated samples developed ASR values below 100 mΩ cm^2, the target value for SOFC applications. The ASR was found to increase in the order: Y_2O_3/Au, Y_2O_3, and Y_2O_3/Co_3O_4.

© 2010 Elsevier B.V. All rights reserved.

1. Introduction

In intermediate-temperature SOFCs – operating in the typical range 600–800 °C – the material of choice for interconnects are ferritic stainless steel grades, AISI 430 in particular. The chief reasons for this material selection are adequate high-temperature mechanical and chemical properties, coefficient of thermal expansion matching the other fuel cell stack components and cost-effectiveness [1]. Nevertheless, the use of this material is not devoid of drawbacks. Specifically, (i) the high Cr content tends to lead to the formation of volatile Cr compounds that end up poisoning the catalysts and (ii) oxides forming on the bare ferritic stainless steel have a relatively low electrical conductivity, resulting in a build-up of series ohmic resistance at each contact. Interconnect durability issues are currently believed to be the single most critical source of cell degradation, limiting the lifetime of planar SOFC systems implementing metallic interconnects [2,3].

An approach towards minimising such disadvantages is resorting to the use of coatings that exhibit the dual action of protecting against high-temperature corrosion in O_2 and preserving a high electrical conductivity of the surface. $La_{1-x}Sr_xMnO_3$ films were deposited by slurry-dipping [4] and plasma-sputtering [5]. Recently, mixed Mn–Co oxide coatings have been fabricated by anodic electrodeposition from Mn^{2+} and Co^{2+} sulphate baths [6]. Good performances were obtained by coatings of yttrium oxide [7,8], mixed yttrium/cobalt oxide [8,9] or mixed yttrium/cerium oxide [9] prepared by sol–gel techniques. Wei et al. [10] electrodeposited composite yttria–Ag coatings from Ag^+ and Y^{3+} nitrate solutions by a multiple-step approach as well as praseodymia coatings from a chloride bath containing PDDA as binder. After thermal treatment at 750 °C the yttrium and praseodymium oxides react with chromium oxide giving rise to the formation of uniform, dense and protective $YCrO_3$ and $PrCrO_3$ perovskite layers, able to prevent the progress of oxidation. Furthermore, contact-resistance measurements have shown that these systems exhibit a low electrical resistance, with limited increase with oxidation time.

Moreover, the electrosynthesis of oxide-based coatings has proved attractive in other fields where the prevention of high-temperature oxidation of stainless steel is required. Electrodeposition of adherent, corrosion resistant Al_2O_3 and Al_2O_3–YSZ coatings has been reported in [11–13] and [13], respectively.

* Corresponding author. Tel.: +39 0832 297323; fax: +39 0832 297111.
E-mail address: benedetto.bozzini@unisalento.it (B. Bozzini).

0378-7753/$ – see front matter © 2010 Elsevier B.V. All rights reserved.
doi:10.1016/j.jpowsour.2010.02.055

In this paper we propose mixed oxide and metal-ceramic composite coatings, obtained by electrodeposition from hydroalcoholic solutions, containing chitosan as binder. The beneficial effects of the use of polymer in solution – allowing to obtain more adherent and less cracked coatings – were discussed in [14] and references therein contained. Briefly, the use of a polymer (such as chitosan) in oxide electrodeposition solutions is a widely documented method to optimise the mechanical properties of the coatings as well as their adhesion to the substrate [14–17]. Incorporation of chitosan in general takes place, owing to precipitation caused by local alkalinisation at the cathode. In fact, deprotonation of the amminic group of chitosan gives rise to a sparingly soluble species that is easily incorporated into the deposits [18]. A similar mechanism is typically involved in the incorporation of other polymer as PEI (polyethylene imine), PVA (polyvinylamine) and PAH (polyallylamine chlorhydrate) into ceramic electrodeposits [19,20]. The incorporation of the polymer within the deposit, leads to an increase of weight-gain rate under otherwise identical electrodeposition conditions [21]. Direct measurements of incorporated chitosan and of its fate during heat treatment shall be published in a subsequent paper. Our coatings have been subjected to prolonged testing at high temperature in O_2 atmosphere and the resulting structure, composition, adhesion and electrical performance have been investigated. Our work in complemented with quantitative information regarding the electrodeposition process.

2. Materials and methods

2.1. Chemicals and electrodes

In this work the following yttria-based coatings were deposited onto AISI 430 ferritic stainless steel samples: (i) pure yttria, (ii) yttria/cobalt oxide compounds, and (iii) yttria/gold composites.

The yttria electrodeposition bath had the following composition: 5 mM $YCl_3{\cdot}6H_2O$ (Acros), 0.15 g L^{-1} chitosan (Aldrich), solvent: CH_3CH_2OH (Carlo Erba) + H_2O (ultra-pure water from a Milli-Q Millipore system, with resistivity higher than 20 MΩ cm) 30 vol.%, CH_3COOH (Carlo Erba) 0.3 vol.%. To this basic bath, 5 mM $CoCl_2{\cdot}6H_2O$ (Carlo Erba) or 5 mM $HAuCl_4{\cdot}3H_2O$ (Aldrich) was added to obtain yttria/cobalt oxide and yttria/gold layers. For comparison, also baths without chitosan were used, where indicated. As cathodes, we used: (i) sheets of AISI 430 stainless steel of thickness 1 mm and areas 4 and 1 cm^2 for the studies of electrodeposition rates and area-specific resistance (ASR), respectively and (ii) Pt (Goodfellow 99.95+%, thickness 250 μm, area 12 cm^2) for the deposition of gram-amounts of powder for XRD investigations of crystallisation kinetics. The counter-electrode was a platinised Ti expanded-mesh electrode of area 20 cm^2. Galvanostatic electrodeposition experiments were performed with an AMEL 5000 potentiostat. The powders were obtained by electrodepositing at 5 mA cm^{-2} for 4 h on a Pt cathode and scraping off the deposit, for subsequent heat treatment. Heat treatments were carried out for 1 h in air at the temperatures detailed in Section 3. Independently prepared replicated powder samples were used, for higher statistical reliability. For comparison, Y/Co powders were electrodeposited from baths without and with chitosan, under otherwise identical conditions, in order to assess any structural effects of the presence of this binder.

2.2. Characterisation of the deposits

The morphology and quantitative composition of the electrodeposits were investigated by SEM ZEISS EVO 50 XVP equipped with EDS INCA ENERGY 200 system. The crystallographic structure of electrodeposited powders – in as-plated and heat-treated conditions – as well as of scales grown onto bare and coated stainless steel samples was determined – as a function of heat-treatment temperature and time – by ex situ XRD, using a Ultima + Rigaku diffractometer, equipped with a Bragg–Brentano goniometer.

The electrical quality of interconnects is typically evaluated ASR, a complex combination of intrinsic (resistivity) and extrinsic (thickness, roughness) material properties as well as of the measurement procedure (applied contact pressure) [22]. The ASR measurement system we employed in this research was constructed in our laboratory and implemented the four-point probe method, with an accessible pressure range of 0.786–10.48 MPa with a high-impedance voltmeter (AMEL 7050) and high-quality current source (AMEL 2049). After an accurate optimisation procedure, we selected the following operating conditions: sample area 1 cm^2, contact force applied by pressing two Cu blocks against the sample, a set of calibration runs with reference materials has demonstrated that the optimal pressure for our investigation is 2.6 MPa. Scratch tests were performed in order to evaluate coating adhesion. Specimens were scratched using a CSM testing machine, mod. MCT/SN 50-0223, with a preload of 1N, load speed of 12.5 N min^{-1} up to a maximum load of 30 N, according to the ASTM C1624 standard. During tests normal and tangential loads were recorded. The scratch line was measured by SEM in order to determine the critical scratch load and allow calculation of the coating shear stress. The coating thickness was estimated from atomic and phase composition data and weight-gain measurements.

3. Results and discussion

3.1. Electrodeposition rate

In order to evaluate coating growth rates, we carried out electrodeposition experiments at 5 and 10 mA cm^{-2} with the three investigated solutions, for times in the range 2–8 min. Weight-gain ΔP (mg cm^{-2}) data are reported in Fig. 1. Three independent weight-gain measurements have been carried out for each electrodeposition condition, on the plots we report the corresponding mean values and standard deviations. The dependence of the growth rate on electrodeposition time conforms to the model proposed in [14], to which the fits reported in Fig. 1 correspond.

3.2. Morphological study by SEM and compositional analysis by EDX

Compositional and morphological characterisation was performed for samples prepared by electrodepositing at 5 mA cm^{-2} for 4 min. The Y and Y/Co deposits exhibit the typical cracked morphology of electrodeposited ceramics [15,23–28], deriving from drying shrinkage: typical micrographs of as-plated and crystallised (heat-treated at 600 °C for 1 hour) Y/Co samples are reported in Fig. 2a and d, respectively. At variance from pure ceramic coatings, the Y/Au composite deposit shows a more compact, micrograined morphology with relatively less extensive cracking and smaller patches visible is the as-plated condition (Fig. 2b and c), but tending to heal after annealing (Fig. 2e and f).

Compositional information on Y/Co and Y/Au samples was obtained by EDX analysis. The Y/Co atomic ratio was 1.1, while the Y/Au atomic ratio was 0.38.

3.3. Structural analysis by XRD

3.3.1. XRD of electrodeposited powders

In Fig. 3 we report X-ray diffractograms recorded with electrodeposited powders of the three investigated types, as well as the Y/Co system prepared without chitosan, for comparison. XRD measurements have been carried out with powders in the as-plated

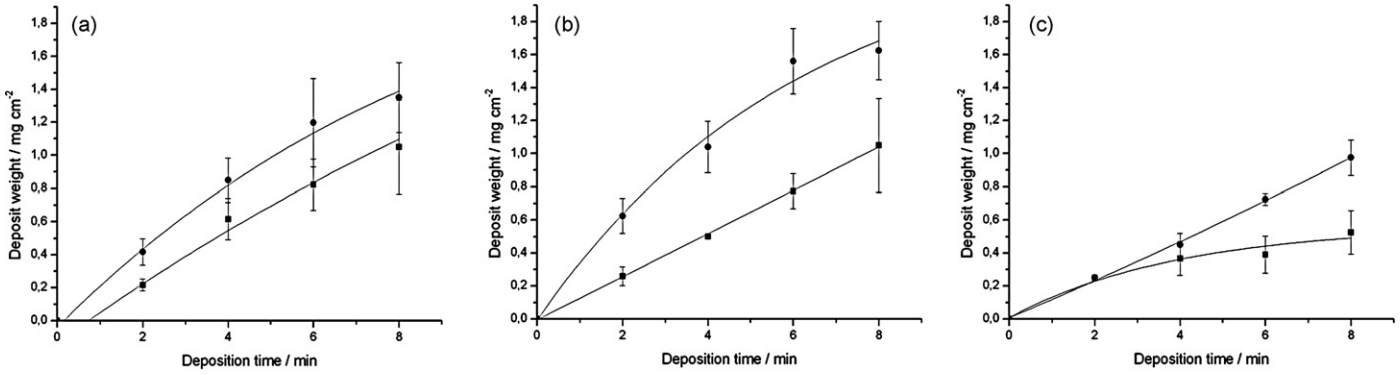

Fig. 1. Weight-gain as a function of deposition time for (a) yttria, (b) yttria/cobalt oxide, and (c) yttria/Au deposits at 5 mA cm^{-2} (■) and 10 mA cm^{-2} (●).

conditions and after heat treatment of 1 h at the indicated temperatures.

The pure yttria powder (see Fig. 3a) is X-ray amorphous in the as-plated conditions and up to 400 °C, exhibiting the typical short-range order ring at ca. 29°, corresponding to a nearest neighbour distance of 1.43 nm. Well-defined diffraction peaks start to appear at 600 °C and crystallisation proceeds in the cubic structure – with progressively better definition and sharpening of the peaks – up to 800 °C. No appreciable structural differences were found between the power electrodeposited in the absence and in the presence of chitosan. This result is coherent with literature reports regarding yttria electrodeposited from aqueous chloride and nitrate solutions [26,29] as well as from hydroalcoholic nitrate solutions [30].

The Co powder (Fig. 3b) starts to crystallise at 300 °C into the cubic Co_3O_4 structure, coherently with the literature results regarding Co_3O_4 in the presence of PEI [31].

The Y/Co powder electrodeposited in the absence of chitosan (see Fig. 3c) starts to crystallise at 300 °C, giving rise to the same cubic Co_3O_4 found in the Co electrodeposits presented above. At higher temperatures, Y_2O_3 peaks appear and the final condition of the heat-treated powder is a two-phase system containing Y_2O_3 and Co_3O_4.

Y/Co powder electrodeposited in the presence of chitosan (see Fig. 3d) exhibits the presence of an additional phase. Replicated measurements performed with two independently electrodeposited batches of powder confirm this outcome. A definitive assignment of the new phase is of course hampered by the presence of other phases with possibly overlapping peaks, but the simplest structure justifying the new diffraction lines seems to correspond to a tetragonal structure with $c/a = 0.86$, as identified by the Bund Abacus approach [32].

3.3.2. XRD of coatings electrodeposited onto AISI 430

XRD spectra for uncoated and coated AISI 430 samples – annealed in air at 800 °C for 500 h – are shown in Fig. 4. The diffractograms of coated samples correspond to films grown by at 5 mA cm^{-2} for 3 min.

In the uncoated sample (Fig. 4a) one can observe the ferrite phase of the substrate and the following oxidation products, known from the literature: $(Cr,Fe)_2O_3$ and $(Mn,Cr)_3O_4$ [8].

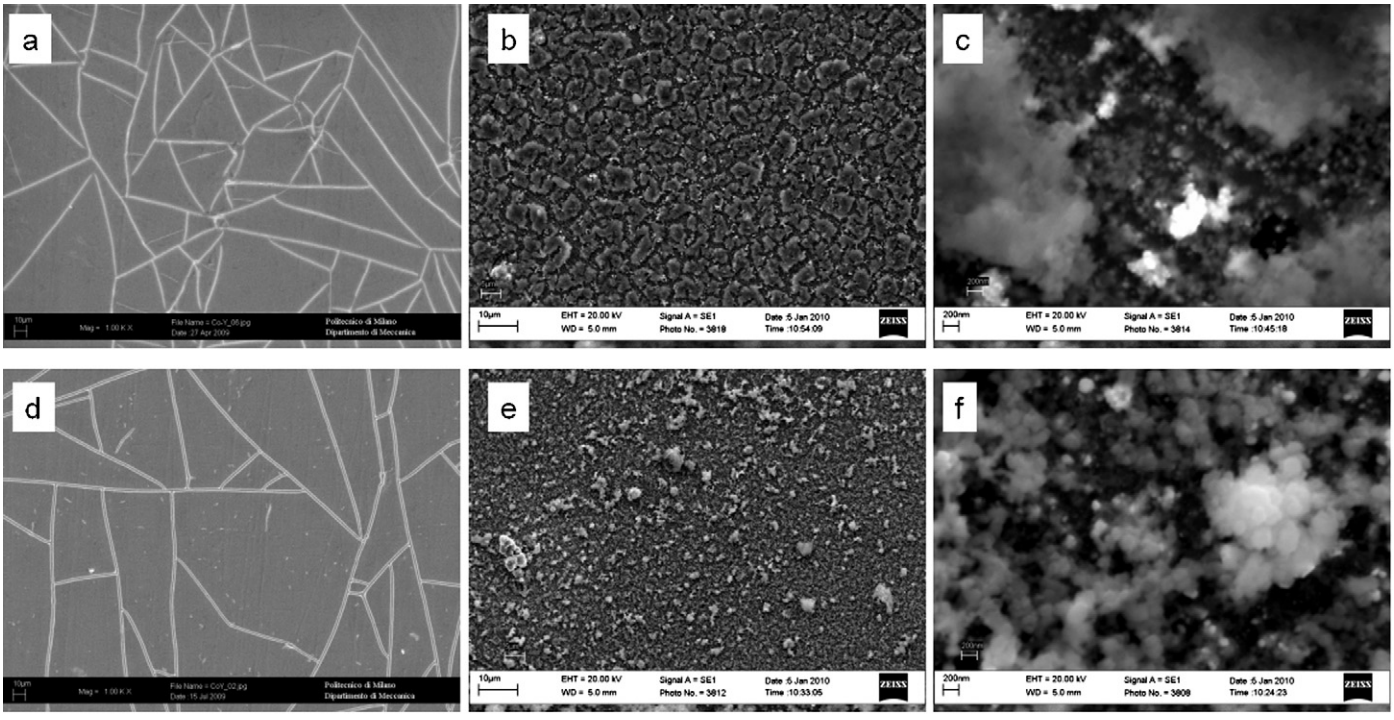

Fig. 2. SEM micrographics of yttria/cobalt oxide (a: as-plated and d: crystallised at 600 °C for 1 h) and yttria/Au (b and c: as-plated, e and f: crystallised at 600 °C for 1 h) deposits obtained at 5 mA cm^{-2}, 4 min. Magnifications: a–e: 1000×; c and f: 20,000×.

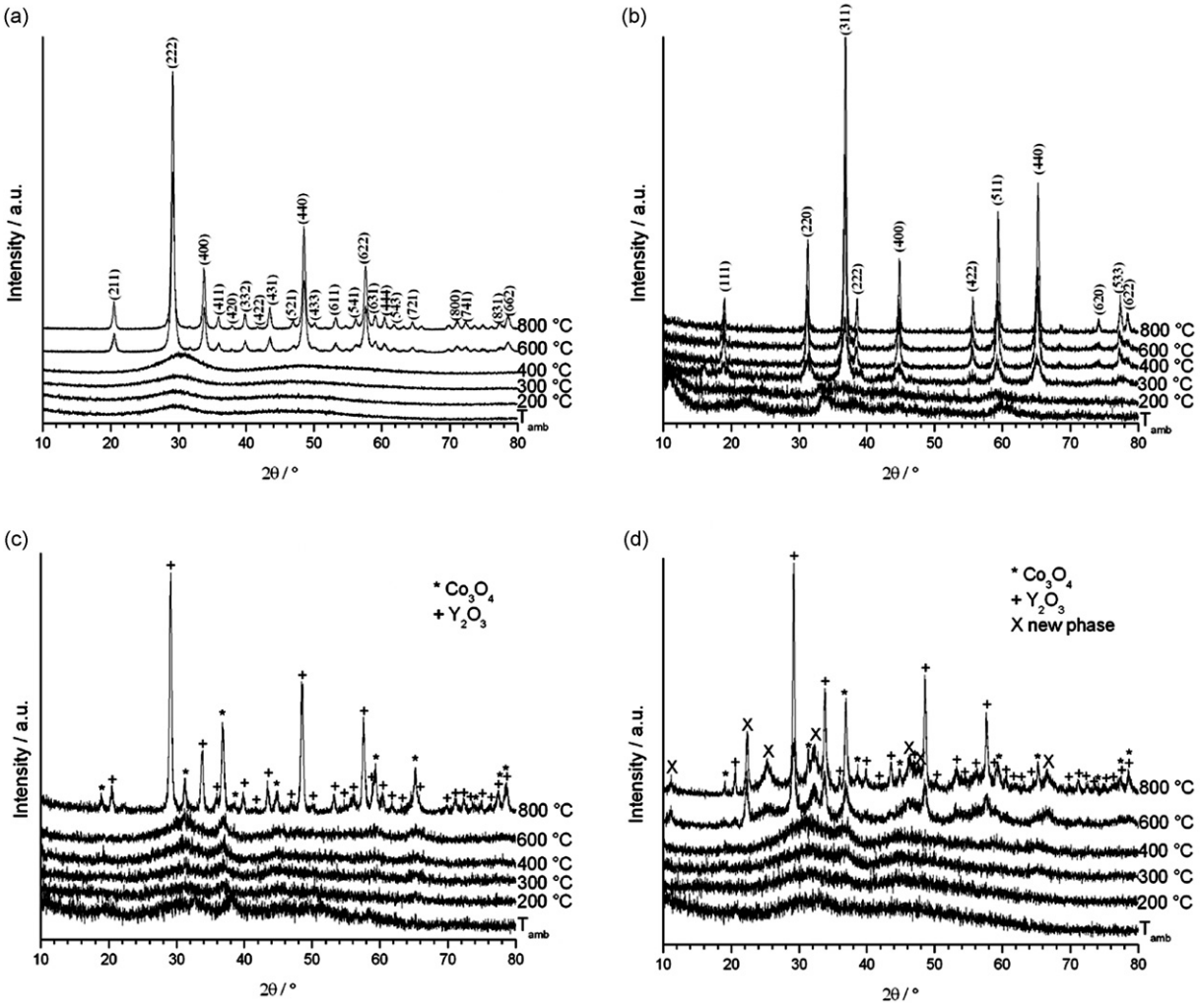

Fig. 3. X-ray diffractograms of powders electrodeposited at 5 mA cm^{-2} for 4 h, as-plated and heat treatment for 1 h at the indicated temperatures. (a) Yttria, (b) cobalt oxide, (c) yttria/cobalt oxide from bath without chitosan, and (d) yttria/cobalt oxide from bath with chitosan.

Samples coated with the pure yttria film (Fig. 4b), also develop the phase $YCrO_3$, forming by diffusion of yttrium into chromia deriving from the substrate, in accord with the literature [10]. The peaks at 30.9 and 28.9° 2θ-CuK$_\alpha$ can be attributed to the phase $YMnO_3$ ((0 0 4) and (1 1 0) respectively), not reported in the literature concerning the oxidation of yttria films grown onto ferritic stainless steel grades. In fact, the other most intense peaks of this phase ((1 1 2) and (1 1 1) [33]) are found in positions overlapping other phases, whose assignment is unambiguous. Coherently with [8,10], no Y_2O_3 was found after high-temperature oxidation of the coating.

With Y–Co coatings (Fig. 4c) neither Y_2O_3 nor Co_3O_4 were detected, but rather $YCrO_3$ is visible, with peaks shifted to higher angles, possibly corresponding to a reduction of unit cell volume, resulting from Cr^{3+} substitution by Co^{3+} [34]. From the literature [8,10] it is known that perovkites hinder Cr diffusion and markedly reduce the formation of volatile Cr compounds. Furthermore, also the spinel reflections are detected, again with a peak shift to higher angles, that can be justified with the formation of the $Mn(Cr,Co)O_4$ phase with Co^{3+} substituting Cr^{3+} [35].

In Fig. 4d we report the XRD spectra corresponding to the Au–Y composite coatings. In addition to the oxidation products of ferritic stainless steel, the $YCrO_3$ phase was found, together with metallic Au reflections.

3.4. ASR measurements

In the literature, a close-knit group of accounts of ASR measurements can be found, regarding candidate coating materials for SOFC metallic interconnects. Wei et al. [10] proposed an Ag/Y_2O_3 electrodeposited coating, obtaining the following results: for the uncoated samples ASR was 200 mΩ cm^2 after 24 h at 750 °C in air and 50 mΩ cm^2 after 168 h at 750 °C. The same material, subjected to a H_2 pretreatment, yielded even better results: ~30 mΩ cm^2. The ASR of Ag/Y_2O_3 coating samples was lower by half than after 24 h and by a factor of 500 after 168 h, compared with uncoated samples. Anodic Mn–Co oxide coatings [6] exhibited ASR of ~60 mΩ cm^2 after 500 h at 800 °C in air. Y and Y/Co oxide coatings, prepared by the sol–gel technique, gave rise to ASR of ~25 mΩ cm^2 after 500 °C at 750 °C in air [8]. Montero et al. [36] investigated $MnCo_{1.9}Fe_{0.1}O_4$ layers prepared by screen-printing, that exhibit ASR values of around 40 mΩ cm^2. Recently, the effects of Mn–Co–Fe spinel dip-coated layers, deposited over Crofer 22H and exposed to air at 800 °C for 400 h have been reported to result in the development of ASR values in the range of 38–63 mΩ cm^2 [37].

Our ASR measurements were carried out for uncoated and coated samples annealed at 800 °C for 1, 250 and 500 h. The coating preparation conditions were 5 mA cm^{-2}, 3 min. The

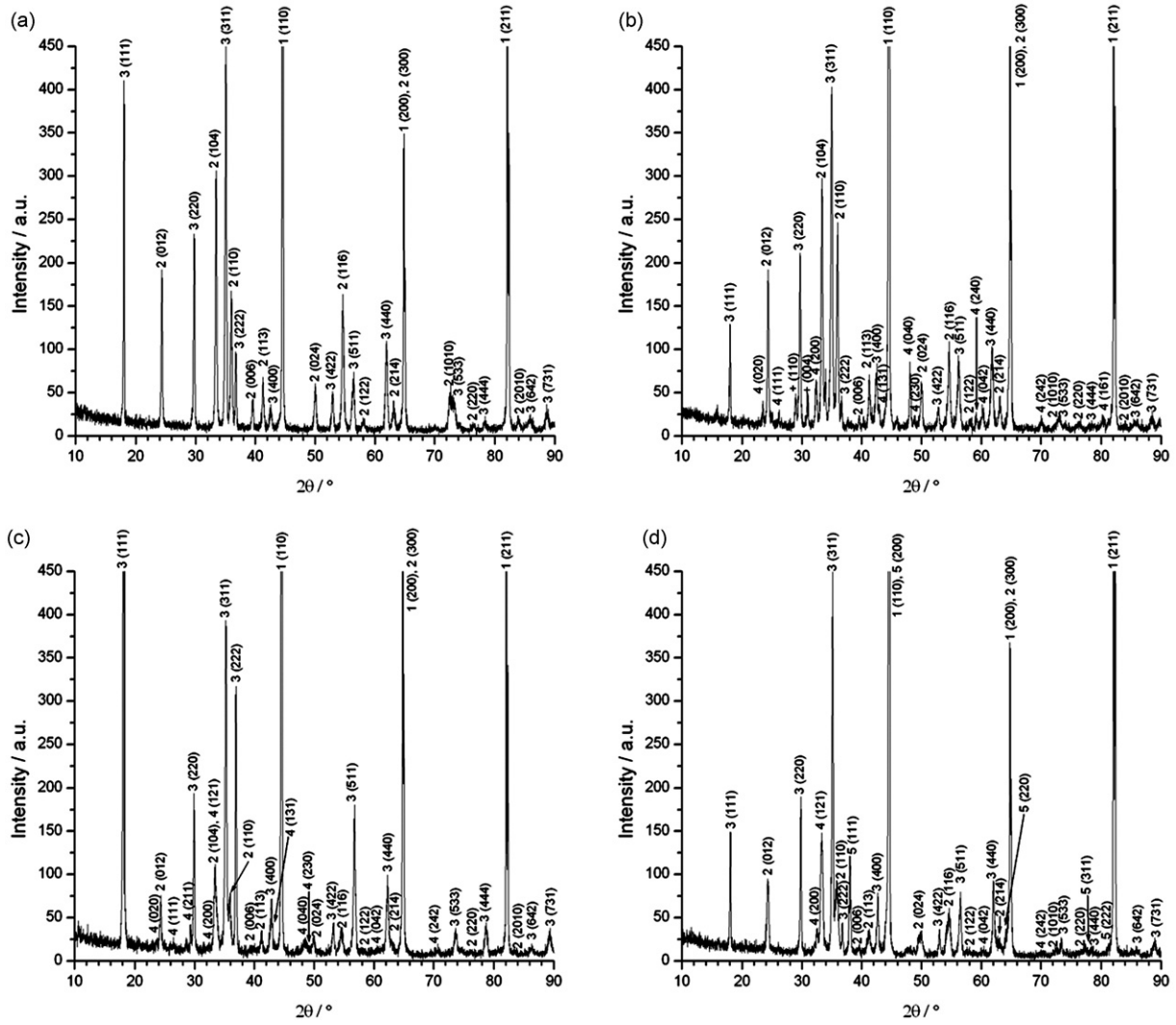

Fig. 4. X-ray diffractograms of uncoated and coated AISI 430 annealed for 500 h at 800 °C. (a) Uncoated specimen (1: ferrite, 2: $(Cr,Fe)_2O_3$, 3: $(Mn,Cr)_3O_4$); (b) yttria coating (1: ferrite, 2: $(Cr,Fe)_2O_3$, 3: $(Mn,Cr)_3O_4$, 4: $YCrO_3$, (+) new phase, attributed to $YMnO_3$); (c) yttria/Co oxide coating (1: ferrite, 2: $(Cr,Fe)_2O_3$, 3: $(Mn,Cr)_3O_4$, 4: $YCrO_3$); (d) yttria/Au coating (1: ferrite, 2: $(Cr,Fe)_2O_3$, 3: $(Mn,Cr)_3O_4$, 4: $YCrO_3$, 5: Au).

deposit thicknesses were yttria $1.2 \pm 0.2\,\mu m$, yttria/Co oxide $1.4 \pm 0.3\,\mu m$, yttria/Au $0.45 \pm 0.08\,\mu m$. Averages of 10 replicated ASR measurements performed on two independently prepared samples and the corresponding standard deviations are reported in Fig. 5. Au-containing composite coatings outperform the other systems, but all the samples electroplated in this research exhibit ASR values below the conventional acceptability limit for SOFC applications of $100\,m\Omega\,cm^2$ [8,10,22].

3.5. Scratch testing

The adhesion of Y/Co and Y/Au deposits was estimated by scratch testing in as-plated (amorphous) and crystallised (heat-treated at 600 °C for 1 h) conditions. All samples (Y/Co: as-plated and heat-treated, Fig. 6a and b, respectively; Y/Au: as-plated and heat-treated, Fig. 6c and d, respectively) exhibit a ductile failure mechanism, with regularly spaced and shaped spallations, caused by delamination mechanisms (wedging spallation according to ASTM C 1624). The following shear stress values were found: Y/Co: 190 MPa as-plated and 135 MPa heat-treated; Y/Au: 260 MPa as-plated and 245 MPa heat-treated.

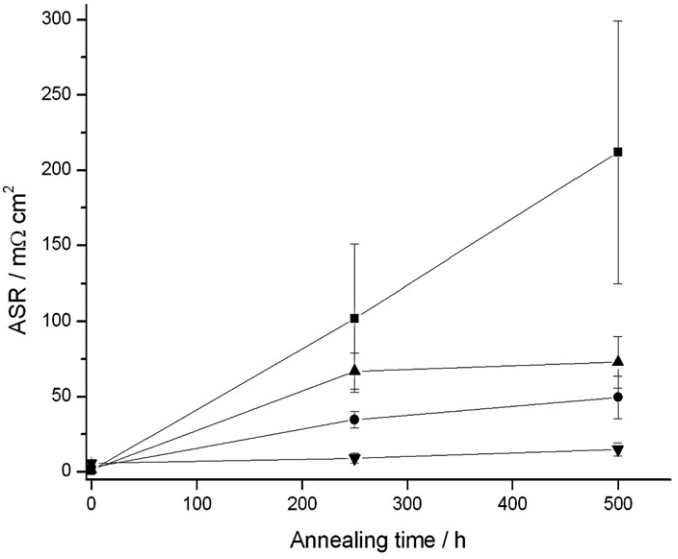

Fig. 5. ASR results for uncoated (■) and coated AISI 430, oxidised in air at 800 °C: yttria (●), yttria/Co oxide (▲) and yttria/Au (▼).

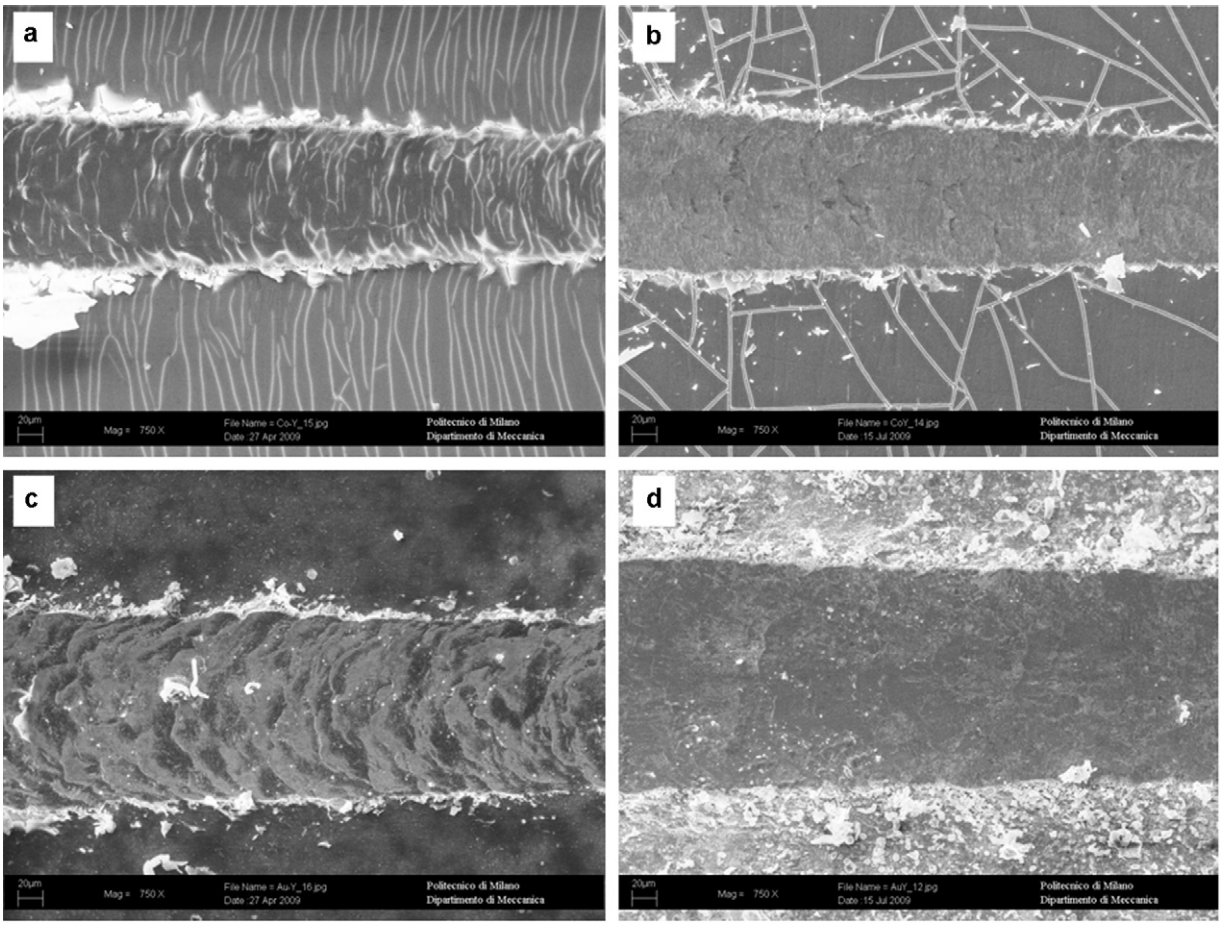

Fig. 6. SEM micrographs (magnification 750×) recorded along AISI 430 samples coated with yttria-based films electrodeposited at 5 mA cm^{-2} for 4 min. (a) Yttria/cobalt as-plated, (b) yttria/cobalt oxide annealed at 600 °C for 1 h, (c) yttria/Au as-plated, and (d) yttria/Au annealed at 600 °C for 1 h.

4. Conclusions

In this work we have proved the feasibility of the electrochemical fabrication yttria-based ceramic coatings for fuel cell interconnects. We studied yttria/Co oxide compound films and yttria/Au composite layers. We employed metal chloride salts in a hydroalcoholic solvent, in the presence of chitosan as a binder, obtaining deposition rates adequate for applications, good bath stability and improving adhesion – in both the as-plated and high-temperature annealed states – as tested by scratch testing. The intrinsic crystalline structure of the electrodeposited materials was investigated, as a function of heat-treatment time, by XRD measurements of electrodeposited powders. Furthermore, the crystal structure of coated AISI 430 foils was studied after oxidation at 800 °C in air for 500 h: typically, mixed oxide phases were formed, containing the electrodeposited materials together with Cr and Mn from the ferritic stainless steel substrate. The Au-containing films developed a composite structure containing metallic Au in conjunction with Y, Cr, and Fe mixed oxides. Eventually, we have demonstrated that the coated samples show ASR values remarkably lower than those of uncoated samples as well as lower than the level recommended in the literature for the relevant application. The most satisfactory results were obtained with Y/Au coatings, showing an ASR increase lower than a factor of 3 after air oxidation at 800 °C for 500 h.

References

[1] L. Chen, Z. Yang, B. Jha, G. Xia, J.W. Stevenson, J. Power Sources 152 (2005) 40–45.
[2] I. Antepara, I. Villarreal, L.M. Rodriguez-Martinez, N. Lecanda, U. Castro, A. Laresgoiti, J. Power Sources 151 (2005) 103–107.
[3] B. Hua, J. Pu, W. Gong, J. Zhang, F. Lu, L. Jian, J. Power Sources 185 (2008) 419–422.
[4] J.H. Kim, R.H. Song, S.H. Hyun, Solid State Ionics 174 (2004) 185–191.
[5] C.L. Chu, J.Y. Wang, S. Lee, Int. J. Hydrogen Energy 33 (2008) 2536–2546.
[6] W. Wei, W. Chen, D.G. Ivey, J. Power Sources 186 (2009) 428–434.
[7] F. Riffard, H. Buscail, E. Caudron, R. Cueff, C. Issartel, S. Perrier, Appl. Surf. Sci. 199 (2002) 107–122.
[8] W. Qu, L. Jian, D.G. Ivey, J.M. Hill, J. Power Sources 157 (2006) 335–350.
[9] W. Qu, L. Jian, D.G. Ivey, J.M. Hill, J. Power Sources 138 (2004) 162–173.
[10] P. Wei, I. Zhitomirsky, A. Petric, in: S.C. Singhal, J. Mizusaki (Eds.), Proceedings of the 9th international symposium on SOFC, The Electrochemical Society Inc, Pennington, NJ, 2005, pp. 1851–1858.
[11] L. Aries, J. Appl. Electrochem. 24 (1994) 554–558.
[12] L. Aries, J. Roy, J. Sotoul, V. Pontet, P. Consteseque, T. Algouy, J. Appl. Electrochem. 26 (1996) 617–622.
[13] S. El Hajjaji, S. Manov, J. Roy, T. Aigouy, A. Ben Bachir, L. Aries, Appl. Surf. Sci. 180 (2001) 293–301.
[14] E. Tondo, M. Boniardi, D. Cannoletta, M. D'Elia, L. D'Urzo, B. Bozzini, Surf. Coat. Technol. 203 (2009) 3427–3434.
[15] I. Zhitomirsky, A. Petric, Mater. Lett. 46 (2000) 1–6.
[16] I. Zhitomirsky, J. Appl. Electrochem. 34 (2004) 235–240.
[17] N. Nagarajan, M. Cheong, I. Zhitomirsky, Mater. Chem. Phys. 103 (2007) 47–53.
[18] I. Zhitomirsky, J. Mater. Sci. 41 (2006) 8186–8195.
[19] I. Zhitomirsky, J. Alloys Compd. 434–435 (2007) 823–825.
[20] A.R. Boccaccini, I. Zhitomirsky, Curr. Opin. Solid State Mater. Sci. 6 (2002) 251–260.
[21] I. Zhitomirsky, A. Hashambhoy, J. Mater. Process. Technol. 191 (2007) 68–72.
[22] W.Z. Zhu, S.C. Deevi, Mater. Res. Bull. 38 (2003) 957–972.
[23] R. Chaim, I. Silberman, L. Gal-Or, J. Electrochem. Soc. 138 (1991) 1942–1946.
[24] R. Chaim, I. Zhitomirsky, L. Gal-Or, H. Bestgen, J. Mater. Sci. 32 (1997) 389–400.
[25] I. Zhitomirsky, R. Chaim, L. Gal-Or, H. Bestgen, J. Mater. Sci. 32 (1997) 5205–5213.
[26] I. Zhitomirsky, A. Petric, J. Mater. Chem. 10 (2000) 1215–1218.
[27] X. Pang, I. Zhitomirsky, M. Niewczas, Surf. Coat. Technol. 195 (2005) 138–146.
[28] S.K. Yen, Mater. Chem. Phys. 63 (2000) 256–262.
[29] R. Siab, G. Bonnet, J.M. Brossard, J.F. Dinhut, Appl. Surf. Sci. 236 (2004) 50–56.

[30] J.M. Brossard, J. Balmain, J. Creus, G. Bonnet, Surf. Coat. Technol. 185 (2004) 275–282.
[31] E.A. McNally, I. Zhitomirsky, D.S. Wilkinson, Mater. Chem. Phys. 91 (2005) 391–398.
[32] A. Guinier, Théorie et technique de la Radiocristallographie, Dunod, Paris, 1956, p. 231.
[33] D. Kim, D. Killingensmith, D. Dalton, V. Olariu, F. Gnadinger, M. Rahman, A. Mahmud, T.S. Kalkur, Ferroelectric properties of $YMnO_3$ films deposited by metal organic chemical vapour deposition on $Pt/Ti/SiO_2/Si$ substrates, Mater. Lett. 60 (2006) 295–297.
[34] H.P.S. Corrêa, C.O. Paiva-Santos, L.F. Setz, L.G. Martinez, S.R.H. Mello-Castanho, M.T. Orlando, Crystal structure refinement of Co-doped lanthanum chromites, Powder Diffract. Suppl. 23 (2008) S18–S22.
[35] Joint Committee on Powder Diffraction Standard, The International Center for Diffraction Data, Card No.: 26-0474.
[36] X. Montero, F. Tietz, D. Sebold, H.P. Buchkremer, A. Ringuede, M. Cassir, A. Laresgoiti, I. Villarreal, $MnCo_{1.9}Fe_{0.1}O_4$ spinel protection layer on commercial ferritic steels for interconnect applications in solid oxide fuel cells, J. Power Sources 184 (2008) 172–179.
[37] M. Alvarez, N. Arizmendiarrieta, I. Villarreal, M. Rivas, Proceedings of the "European Fuel Cell Tecnhnology & Applications—Piero Lunghi Conference" EFC09, Rome, December 15–18, 2009, Paper #17097.